JOURNAL OF GEOPHYSICAL RESEARCH, VOL. 114, F04019, doi:10.1029/2008JF001191, 2009

Hindcasting of decadal-timescale estuarine bathymetric change with a tidal-timescale model

Neil K. Ganju,[1,2,3] David H. Schoellhamer,[1,2] and Bruce E. Jaffe[4]

Received 12 November 2008; revised 10 August 2009; accepted 27 August 2009; published 2 December 2009.

[1] Hindcasting decadal-timescale bathymetric change in estuaries is prone to error due to limited data for initial conditions, boundary forcing, and calibration; computational limitations further hinder efforts. We developed and calibrated a tidal-timescale model to bathymetric change in Suisun Bay, California, over the 1867–1887 period. A general, multiple-timescale calibration ensured robustness over all timescales; two input reduction methods, the morphological hydrograph and the morphological acceleration factor, were applied at the decadal timescale. The model was calibrated to net bathymetric change in the entire basin; average error for bathymetric change over individual depth ranges was 37%. On a model cell-by-cell basis, performance for spatial amplitude correlation was poor over the majority of the domain, though spatial phase correlation was better, with 61% of the domain correctly indicated as erosional or depositional. Poor agreement was likely caused by the specification of initial bed composition, which was unknown during the 1867–1887 period. Cross-sectional bathymetric change between channels and flats, driven primarily by wind wave resuspension, was modeled with higher skill than longitudinal change, which is driven in part by gravitational circulation. The accelerated response of depth may have prevented gravitational circulation from being represented properly. As performance criteria became more stringent in a spatial sense, the error of the model increased. While these methods are useful for estimating basin-scale sedimentation changes, they may not be suitable for predicting specific locations of erosion or deposition. They do, however, provide a foundation for realistic estuarine geomorphic modeling applications.

Citation: Ganju, N. K., D. H. Schoellhamer, and B. E. Jaffe (2009), Hindcasting of decadal-timescale estuarine bathymetric change with a tidal-timescale model, *J. Geophys. Res.*, *114*, F04019, doi:10.1029/2008JF001191.

1. Introduction

[2] Conceptually, simulating decadal-timescale bathymetric change in an estuary may be achieved by modeling hydrodynamics and sediment transport at the tidal timescale. However, small errors in a model calibrated to tidal-timescale data can accumulate over decadal timescales to give unrealistic results for bathymetric evolution [*Schoellhamer et al.*, 2008]. A practical solution is a multiple-timescale calibration method, which involves calibrating to data of different timescales. These calibration procedures give confidence in both the formulation and the application of the model. Due to the difficulty and expense of data collection, however, sufficient calibration data are typically not available.

[3] Early discussion of morphological modeling [e.g., *de Vriend et al.*, 1993; *Latteux*, 1995] highlighted the need for input reduction (reducing the full set of input data to a limited set of cases) not only for computational efficiency, but for robustness of the simulation. Representative sets of forcing data must be selected because measured data (e.g., tides, winds) are unavailable in the future and limited in the past. *Latteux* [1995] identified the concept of a "morphological tide": a temporally reduced set of tidal forcing that creates the same morphological change as the full tidal forcing time series. Due to the importance of freshwater flows and watershed sediment supply in estuarine environments, input reduction is needed for these signals in addition to tides and winds. A limited set of freshwater hydrographs that produce the same morphological change as the actual hydrographs, for example, would constitute "morphological hydrographs."

[4] Several idealized case studies have emerged in recent years, using the concepts of input reduction, representative forcings, and idealization. *Hibma et al.* [2003] modeled the evolution of an idealized estuary over 100 years, recreating patterns of channel-shoal interaction, while *Roelvink* [2006] focused on the implementation of the bed-updating routines and their effect on the evolution of an idealized tidal inlet. *Lesser et al.* [2004] reviewed the development, validation, and testing of a three-dimensional geomorphic model, including a comparison of model performance with bathymetric data near a modified harbor. These studies use the

[1]U.S. Geological Survey, Sacramento, California, USA.
[2]Department of Civil and Environmental Engineering, University of California, Davis, California, USA.
[3]Now at U.S. Geological Survey, Woods Hole, Massachusetts, USA.
[4]U.S. Geological Survey, Santa Cruz, California, USA.

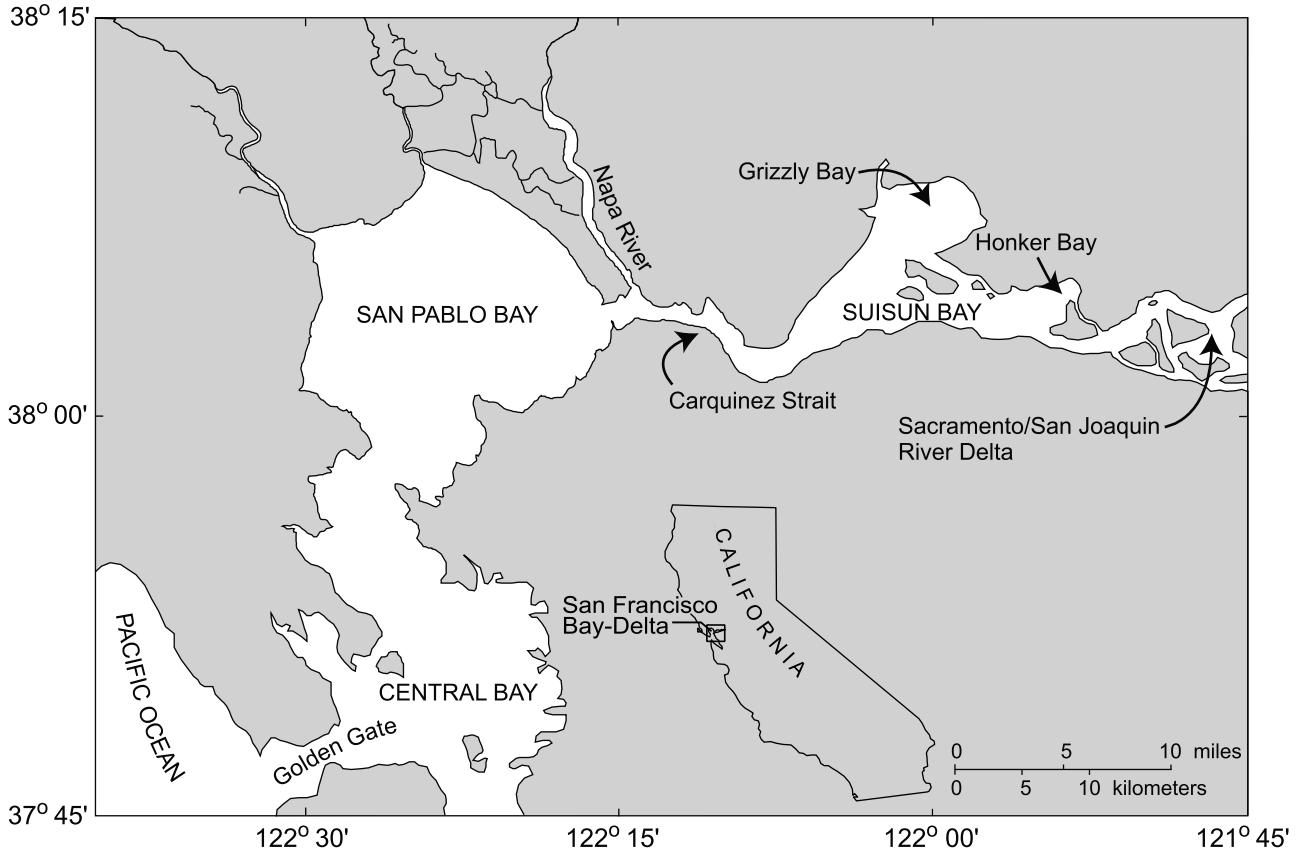

Figure 1. San Francisco Bay, and subembayments Central Bay, San Pablo Bay, and Suisun Bay. Suisun Bay is the landwardmost subembayment, adjacent to the Sacramento and San Joaquin River Delta.

concept of the morphological acceleration factor, whereby the modeled sediment fluxes to and from the bed (and associated bed level change) over a model time step are accelerated linearly. The bed elevation change, bed composition, and water depth are then updated with the scaled value. Further work is needed on the scaling of morphological acceleration in idealized episodic estuarine systems, as has already been done for idealized tidal systems [*Roelvink*, 2006]. Prior realistic modeling efforts have not performed multiple timescale calibrations, tested the use of morphological acceleration with a comparison to observed bathymetric change, or evaluated the efficacy of morphological hydrographs.

[5] Suisun Bay, California (Figure 1), provides an ideal test case, due to the availability of data over multiple timescales and the relative importance of freshwater flow and sediment supply. We apply a tidal-timescale hydrodynamic model, conventionally calibrated at the tidal and annual timescales, to decadal-timescale bathymetric change. The model is applied for the 1867–1887 period, when hydraulic mining released large quantities of sediment to Suisun Bay, and the bathymetric changes were quantified. We compare the modeled bathymetric changes to observations, and evaluate the performance of the model and input reduction techniques.

2. Site Description

[6] Suisun Bay is the landwardmost subembayment of San Francisco Bay, extending from the Sacramento and San Joaquin River Delta at the landward end to Carquinez Strait at the seaward end (Figure 1). Tides are mixed semidiurnal, with a maximum range of 2 m. Over one half of Suisun Bay is shallower than 5 m at mean-lower-low-water (MLLW), though numerous deep-water (>10 m) channels run longitudinally through the bay. Two large shallow areas, Grizzly and Honker Bays, lie on the northern edge of the main channels. Suspended sediment transport within Suisun Bay follows a seasonal cycle: the majority of suspended sediment is delivered through the delta during the large, winter freshwater flows; a portion deposits in the delta, while the remaining sediment is exported through Suisun Bay, to San Pablo Bay. During the following summer months reliable onshore winds generate wind waves, resuspending bed sediments in both Suisun and San Pablo Bays. Due to the greater extent of shallows in San Pablo Bay, there is a gradient of suspended sediment concentration (SSC) from west to east (between San Pablo and Suisun Bays) and, with landward near-bed flows (gravitational circulation), these combine to transport sediment landward into Suisun Bay [*Krone*, 1979; *Ganju and Schoellhamer*, 2006]. *Warner et al.* [2004] detailed the presence of flood tide pulses during low tides which also promote landward flux of sediment into Grizzly Bay.

[7] *Cappiella et al.* [1999] modeled bathymetric surveys of Suisun Bay performed in 1867, 1887, 1922, 1942, and 1990, on to 25 m grids. A continuous surface representation (surface grid) of each bathymetry survey was created from depth soundings and contours using Topogrid, an ArcInfo

module that utilizes a discretized thin plate, spline interpolation technique [*Wahba*, 1990]. Each historical bathymetric surface is defined by more than 200,000 grid cells, and changes in erosion and deposition were computed by differencing surfaces. During the 1867–1887 period, increased sediment supply from hydraulic mining caused an average of 0.03 m/yr deposition in Suisun Bay and Carquinez Strait. In Suisun Bay alone, average deposition was 0.02 m/yr. Notably, the 1867–1887 bathymetric change grid is the only one which contains Grizzly Bay, the largest off-channel shoal area in Suisun Bay (Grizzly Bay was not surveyed in 1922 and 1942). Grizzly Bay occupies roughly 30% of Suisun Bay, and 50% of the shallowest 2 m of Suisun Bay. The 1867–1887 period provides the best test for the model technique for multiple reasons: (1) the initial bathymetric condition is known over the entire domain; (2) the signal from watershed sediment supply is the largest; and (3) it is the obvious starting point for subsequent modeling of the remaining bathymetric change observations.

3. Calibration, Confirmation, and the Multiple-Timescale Approach

[8] Calibration denotes the tuning of model parameters to match observed data or an analytical solution [e.g., *Oreskes et al.*, 1994; *Roache*, 1997; *Cunge*, 2003]. Confirmation, often referred to as validation, is the process of proving the calibrated model is capable of accurately simulating another variable to which it was not calibrated, or accurately simulating a different temporal period. *Cunge* [2003] proposes a modified process, which essentially bundles the calibration and confirmation stages. The purpose of this "modified paradigm" is to eliminate the traditional calibration process, which can lead to model "tweaking," with little attention to physical processes. As *Cunge* [2003] points out, the difference between modeled and observed behavior should be discussed in light of parameter space and physical mechanisms.

3.1. Tidal-Timescale Calibration and Confirmation

[9] The model implemented in the present study was first calibrated and confirmed with modern tidal-timescale data [*Ganju and Schoellhamer*, 2008] to investigate dynamics of the estuarine turbidity maximum (ETM). The ETM is the location of near-bed, convergent sediment transport, which usually causes accumulation of sediment and thereby affects geomorphology. In that study, we calibrated the model to tidal water levels at multiple locations, and confirmed by qualitatively comparing observed and modeled tidal changes in longitudinal and vertical salinities. Boundary conditions consisted of measured water levels and sediment concentrations at the seaward boundary, and bottom friction was the only free parameter. Model results demonstrated the correct salinity structure, with increased stratification during neap tides. The final outcome was a qualitative comparison of observed and modeled movement of the ETM. Proper representation of the ETM gave confidence in the model's ability (in terms of physics and discretization) to reproduce tidal-timescale phenomena that may affect longer-term processes in the estuary.

3.2. Annual-Timescale Calibration and Confirmation

[10] The annual-timescale simulations [*Ganju and Schoellhamer*, 2009] tested the model's ability to represent interannual sediment transport features. In that study, we calibrated and confirmed with five years of tidally averaged sediment flux data [*Ganju and Schoellhamer*, 2006], using a portion of the data for calibration, and the remaining portion for confirmation. The only parameter varied between this step and the prior step was the distribution of two sediment classes. This step established the model's ability to represent sediment delivery from large flow events, landward transport of sediment due to gravitational circulation, and the effect of wind waves on the net sediment budget in the estuary. Decadal-scale changes in these patterns will accumulate to determine decadal-scale geomorphology in the estuary. For example, a decade-long drought would greatly reduce sediment delivery to the estuary and perhaps cause net erosion over that decade. Major changes between this step and the previous tidal-timescale modeling step were the addition of wind waves and an idealized seaward SSC condition (necessary due to a lack of data). The model domain, discretization, and bottom boundary condition were consistent between these two steps.

3.3. Decadal-Timescale Calibration

[11] The final model evaluation step, presented here, involves the decadal-timescale modeling of estuarine bathymetric change. Bathymetric data in Suisun Bay are temporally sparse and spatially dense, but span periods in which system behavior was highly variable (due to rapid changes in sediment supply, land use, and bathymetry itself). In this case, confirmation is not an option. There is large uncertainty in the conditions of the system during historical periods. For example, calibration to one set of parameters for the first time period (1867–1887), may be successful, but confirming to the next time period, 1887–1922, may fail. This could be attributed entirely to a real change in sediment bed parameters during that time. For example, bed erodibility over decadal timescales can be affected by invasive benthic species, changes in biological community structure, and changes in source sediments [*Corenblit et al.*, 2008; *Droppo et al.*, 2007; *Escapa et al.*, 2007].

3.4. Consistency Over Multiple Timescales

[12] The multiple-timescale calibration procedure is critical for developing models of any system. Confidence must be built in the model's ability to simulate short-timescale processes before attempting to simulate long-timescale processes. Short-timescale processes accumulate to alter long-timescale features: for example, ETM formation at the tidal timescale can generate morphological features within estuarine shoals and channels. Those features can then be reworked by interannual wind waves, or nourished by episodic watershed sediment delivery, both of which are annual-timescale processes. Over several years of varying climatic conditions, geomorphology can be altered over the decadal timescale.

[13] The model is consistent at all timescales in the sense that the model physics and discretized domain are unchanged between these exercises. It is necessary to modify boundary conditions due to a lack of data during historic and future periods; we attempted to test the use of these

Table 1. Model Parameters for Decadal-Timescale Simulations

Model Parameter	Value
Number of x direction cells, size range	160, 72–394 m
Number of y direction cells, size range	87, 102–593 m
Number of z direction cells	4
Baroclinic time step	40 s
Barotropic time step	2 s
Simulation steps	788400
Settling velocity	0.10/0.25 mm s^{-1}
Erosion rate	2×10^{-5} kg m^{-2} s^{-1}
Bed critical shear stresses[a]	0.15/1.05 N m^{-2}
Porosity	0.60
Bed density[a]	2000 kg m^{-3}
Initial bed thickness	2.0 m
Wave period[a]	1.425 s
Wave fetch	20 km
Water depth (for wave model)	evolving bathymetry
Tidal boundary velocity, stage	Flather (radiation)
river boundary velocity, stage	Flather (radiation)
Tidal boundary tracers	clamped
River boundary tracers	clamped
Morphological acceleration factor	20

[a]Values were varied for calibration.

conditions by applying them during modern periods with relevant field data (e.g., idealized seaward SSC during the annual-timescale sediment flux simulations). Changes in bed parameters (including critical erosion shear stress and sediment distribution) are warranted due to episodic changes in sediment delivery from the watershed (i.e., hydraulic mining) and the introduction of numerous benthic invasive species during the 19th and 20th centuries [*Carlton et al.*, 1990].

4. Hydrodynamic/Sediment Transport Model

[14] The Regional Ocean Modeling System (ROMS) [*Shchepetkin and McWilliams*, 2005] is a public domain hydrodynamic model. The version discussed here is the Rutgers 3.0 version. In the following section we describe the relevant equations that are solved by the numerical code, but the full details are beyond the scope of this work. Complete details, as well as the open source code itself, can be found at www.myroms.org. Modeling details specific to this application are detailed in section 5. ROMS solves the 3D Reynolds-averaged Navier-Stokes momentum equations, with a finite difference approach. Extensive details are given by *Shchepetkin and McWilliams* [2005]. The generic length scale turbulence closure [*Umlauf and Burchard*, 2003; *Warner et al.*, 2005b] is available; we use this approach to specify the k-ε turbulence closure.

[15] ROMS is applied in conjunction with the Community Sediment Transport Modeling System (CSTMS) [*Warner et al.*, 2008], which has the capability of simulating multiple size classes and bed layers; each size class is transported as an independent quantity. Suspended sediment transport is calculated with the advection-diffusion equation. A source term representing bed erosion is given by *Ariathurai and Arulanandan* [1978] as

$$C_{\text{source}} = \varepsilon_s(1-n)\left(\frac{\tau_w}{\tau_c} - 1\right) \quad \text{for } \tau_w > \tau_c \tag{1}$$

where ε_s is the erosion rate constant, n is the bed porosity, τ_w is the shear stress exerted on the bed, and τ_c is the critical shear strength of the sediment bed. The sediment sink term, deposition, is given by

$$C_{\text{sink}} = \frac{\partial w_s C}{\partial s} \tag{2}$$

where w_s is the bulk settling velocity of the size class (the differential operator is required due to the s coordinate system). Multiple bed layers may be specified, with each layer composed of a user-specified mixture of sediment classes. The properties of the mixed class bed, such as shear strength, are weighted using the average mass fractions of the classes. The details of the bed layer model are given by *Warner et al.* [2008]. Calculation of bed stresses is performed using wave-current interaction [*Madsen*, 1994], as implemented by *Warner et al.* [2008]; they detail the bottom boundary layer module and the other modes available. Wave-generated bottom orbital velocities are specified by providing spatially and temporally varying significant wave heights, directions, and periods. Bottom orbital velocities are calculated using the approximation of *Dean and Dalrymple* [1991] within the bottom boundary layer module. Specification of wave height, direction, and period is discussed in section 5.

[16] In suspended load simulations with no bed load transport, such as this study, the morphological acceleration factor is multiplied against the erosive or depositional flux (equations (1) and (2)) at the bed-water interface. This scales up the evolution of bed change, but does not alter suspended sediment concentrations within the water column (and therefore conserves sediment mass). The change in bed composition is also amplified, as each size class is removed or deposited at the accelerated rate.

5. Hindcast Methods

[17] Model parameters (Table 1) for these simulations were varied to obtain the best agreement with the net bathymetric change data of *Cappiella et al.* [1999]; the use of bathymetric updating and morphological acceleration led to modification of the constant wave period applied by *Ganju and Schoellhamer* [2009], while in-delta sediment storage must be calibrated to match historical data. This was achieved by modifying sediment characteristics and spatial distribution of the two sediment size classes.

5.1. Modeling Domain

[18] The modeling domain of Suisun Bay was constrained between Carquinez Strait on the seaward end and the delta on the landward end (Figure 2). The domain was discretized into a 160 × 87 × 4 cell domain (in the west-east, north-south, and vertical directions, respectively). The vertical resolution was reduced (from 8 to 4 vertical levels) from annual simulations due to computational expense, but the model still reproduced landward near-bed flow, and seaward near-surface flow as observed. The delta was idealized as a single, continuous channel, as described by *Ganju and Schoellhamer* [2008, 2009]. This idealization did not affect tidal or annual timescale hydrodynamic and sediment transport processes within Suisun Bay. The Suisun Bay bathymetric grids of *Cappiella et al.* [1999] were interpolated to a curvilinear, orthogonal grid of the same

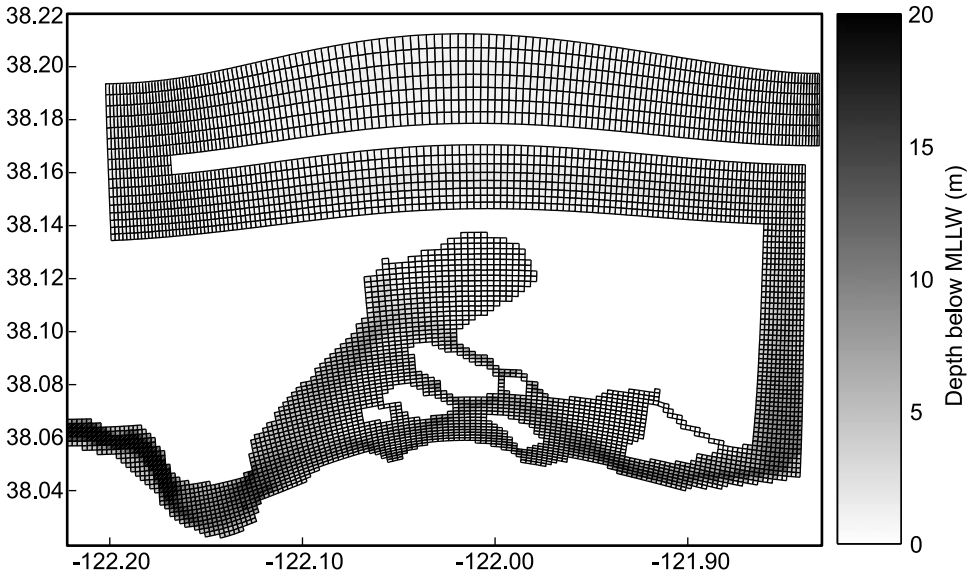

Figure 2. Model domain for hindcasting simulations beginning in 1867; masked cells (land) are not shown.

resolution as was used in the previous modeling efforts. The shape, depths, and trapping efficiency of the actual delta have varied over the last 150 years [*Thompson*, 1957], though there are no detailed data of this type.

5.2. Boundary Conditions

5.2.1. Landward Boundary Conditions: Freshwater Flow, Salinity, SSC

[19] Daily flow and sediment load data to the Sacramento/San Joaquin River Delta are available after 1930 and 1959, respectively, but hindcasting prior to this requires a method to generate daily sediment load estimates into the delta. *Ganju et al.* [2008] developed a daily time series of freshwater flow and sediment load using two historical proxies, monthly rainfall and unimpaired flow magnitudes, to generate monthly unimpaired flows to the Sacramento/San Joaquin Delta for the 1851–1929 period. These historical monthly flows were compared to a limited set of unimpaired monthly flows from 1967 to 1987 [*Knowles*, 2002] and a least squares metric selected a modern year analog for each historical year. The daily hydrograph for the modern analog was then assigned to the historical year and scaled to match the flow volume estimated by dendrochronology methods [*Meko et al.*, 2001, 2002]. *Ganju et al.* [2008] then applied a sediment rating curve to this time series of daily flows, to generate daily sediment loads for 1851–1958. The rating curve was calibrated with the bulk historical load estimates of *Gilbert* [1917] and *Porterfield* [1980]. Extensive details of this procedure are given by *Ganju et al.* [2008]. Use of these bulk load estimates, some of which are based on bathymetric change, does not automatically ensure perfect modeling of bathymetric change: there is potential loss of sediment at the seaward boundary, and also storage/erosion in other domains of the model that have no bathymetric data (e.g., the delta).

5.2.2. Seaward Boundary Conditions: Tidal Velocity, Salinity, SSC

[20] Following *Ganju and Schoellhamer* [2009], a tidal predictor was used for seaward boundary conditions. The tidal elevation and depth-averaged velocity were applied uniformly in a lateral sense at the seaward boundary. Though depth-averaged velocity is not expected to be laterally uniform at the seaward boundary, the configuration and bathymetry of Carquinez Strait modulate those profiles before affecting Suisun Bay.

[21] For seaward salinity, the method of *Warner et al.* [2005a] was used. Flood tide salinity is calculated based on freshwater outflow; this analytical function and the site-specific coefficients are described in detail by *Ganju and Schoellhamer* [2009]. In that study, we demonstrated that salinity gradient was strongly dependent on freshwater outflow; changes in bathymetry are expected to induce a second-order effect and are not considered. *Ganju and Schoellhamer* [2009] demonstrated the efficacy of the boundary salinity function: longitudinal and vertical salinity dynamics in Suisun Bay were reproduced, as was gravitational circulation in Carquinez Strait.

[22] *Ganju and Schoellhamer* [2009] developed a synthetic SSC boundary condition based on measured flood tide SSC at Carquinez Strait landward of the Napa River [*Buchanan and Ganju*, 2005]. The following three signals were superimposed to recreate a synthetic time series of SSC: a freshwater flow signal, a seasonal wind wave signal, and a spring neap signal that is a function of tidal energy (obtained from tidal harmonics). The time series was then modulated by a mean yearly SSC which is linearly related to total sediment input from the delta during the water year. The time series was formulated as

$$SSC_f = \frac{SSC_{CAR}}{2}\left[1 + \cos\left(\frac{2\pi t}{365}\right)\right] \tag{3}$$

$$SSC_w = 100 + 50\left(\cos\frac{2\pi(t+200)}{365}\right) \tag{4}$$

$$SSC_{sn} = a_1\sqrt{SSC_f + SSC_w}(u_{rms} - a_2)^{a_3} \quad (5)$$

$$SSC_{comb} = SSC_f + SSC_w + SSC_{sn} \quad (6)$$

$$SSC = SSC_{comb} + 0.1(rand(0,1))SSC_{comb} \quad (7)$$

where SSC_f, SSC_w, SSC_{sn}, SSC_{comb}, and SSC are the flow, wind, spring neap, combined, and final SSC signals in mg/L; a_1, a_2, and a_3 were varied to yield the best agreement with measured data [*Ganju and Schoellhamer*, 2009] (final values were 300, 0.5, and 2.6 respectively); and t is the time in days. As a measure of tidal energy, we used u_{rms}, the root-mean-square value of velocity at the seaward end of Carquinez Strait, obtained from the tidal predictions mentioned above. SSC_{CAR} is the yearly mean SSC at Carquinez Strait [*Buchanan and Ganju*, 2005], and was regressed against total sediment load from the delta (for the period 1998–2004), yielding:

$$SSC_{CAR} = 69.9Q_s - 16 \quad (8)$$

where Q_s is the total sediment load from the Sacramento and San Joaquin Rivers in millions of tons (Mt). This function represents sediment delivered seaward past Suisun Bay to San Pablo Bay during the high-flow season, and then transported landward to Suisun Bay via gravitational circulation during the low-flow season [*Ganju and Schoellhamer*, 2006]. The second term in equation (7) is a random fluctuation of 10%, representing noise (characteristic in estuarine SSC time series). The final time series essentially represents a tidally averaged SSC signal, which peaks during periods of high wave and tidal energy. The SSC value was assigned equally to two sediment classes: a finer fraction (with low critical shear stress) and a coarser fraction (with higher critical shear stress), with the same properties as assigned to the bed fractions in Suisun Bay and the delta (discussed below). Use of this synthetic condition should not affect formation of the estuarine turbidity maximum in Carquinez Strait, though it may modulate the spatial extent and SSC within the ETM.

5.2.3. Sediment Bed Parameters

[23] As in the previous calibration studies, the sediment bed parameters such as critical shear stress must be used as calibration parameters. There are no data concerning historical sediment bed composition, so we began with the same values as the previous study [*Ganju and Schoellhamer*, 2009], and modified as necessary (Table 1).

5.2.4. Atmospheric Forcing

[24] Spectral analysis of hourly winds in Suisun Bay shows three predominant wind frequencies: diurnal, quasi-weekly (~8 days), and yearly. The yearly signal is attributed to the steady onshore winds during the summer, which peak between June and August. Winter winds are usually associated with episodic Pacific storms. During the summer months, quasi-weekly and diurnal wind signals result from the solar warming and cooling of the Central Valley air mass, leading to periods of strengthened landward winds. A synthetic time series was developed using the following three signals:

$$U_s = a_w\left(1 + \cos\frac{2\pi(t+182)}{365}\right) \quad (9)$$

$$U_w = b_w\left(\frac{U_s}{3} + \cos\frac{2\pi t}{8}\right) \quad (10)$$

$$U_d = c_w\cos(2\pi(t+0.5)) \quad (11)$$

$$U_f = U_s + U_w + U_d - 1 \quad (12)$$

where U_s, U_w, U_d, and U_f are the seasonal, quasi-weekly, daily, and final wind time series, and $a_w = 2.75$, $b_w = 2$, and $c_w = 2$. The wind speed was provided to the model, which then calculated wave height using the Shore Protection Manual method [*Coastal Engineering Research Center*, 1984]. For simplicity, wave direction was held constant at 270°, which is the predominant wind direction. Conceptually, this provides a simple resuspension mechanism in Honker and Grizzly Bays during the summer wind wave season.

5.3. Idealized Time Stepping: Morphological Hydrograph and Morphological Acceleration Factor

[25] For historical simulations (when actual hydrographs are not available), the aforementioned matching procedure of *Ganju et al.* [2008] selected a representative hydrograph (morphological hydrograph) from a limited set of modern data. Once a limited set of modern hydrographs was identified and matched to historical years, each morphological hydrograph was used as input for a 1 year simulation, using initial bathymetry. The bathymetric changes for each year were scaled up based on the occurrence rate of each prototype in the record. For the 1867–1887 period, the matching procedure selected the modern analog years 1969, 1975, and 1978 four times each (Figure 3). Further details of the hydrograph selection procedure are given by *Ganju et al.* [2008].

[26] The other essential modification is the use of a morphological acceleration factor (MF) [*Lesser et al.*, 2004; *Roelvink*, 2006], which accelerates bed changes within the model. Details of the CSTMS implementation are given by *Warner et al.* [2008]. At each time step, the calculated bed sediment fluxes were scaled up by the factor, to produce an accelerated bed change. By using a factor of 20, for example, the changes over one tidal cycle now represented the changes over 20 tidal cycles; changes over one year now represented the changes over 20 years; and feedback between the morphology and hydrodynamics were not ignored (as would be the case with an offline extrapolation). In episodic systems such as this, however, it cannot be assumed that 20 years of simulation, with MF = 1 yields the same result as 1 year of simulation with MF = 20. The present calibration step established the validity of using MF = 20 with a 1 year simulation to represent 20 years of bathymetric change. Ideally, a range of MF from 1 to 20 would be prescribed for a range of times from 20 years to

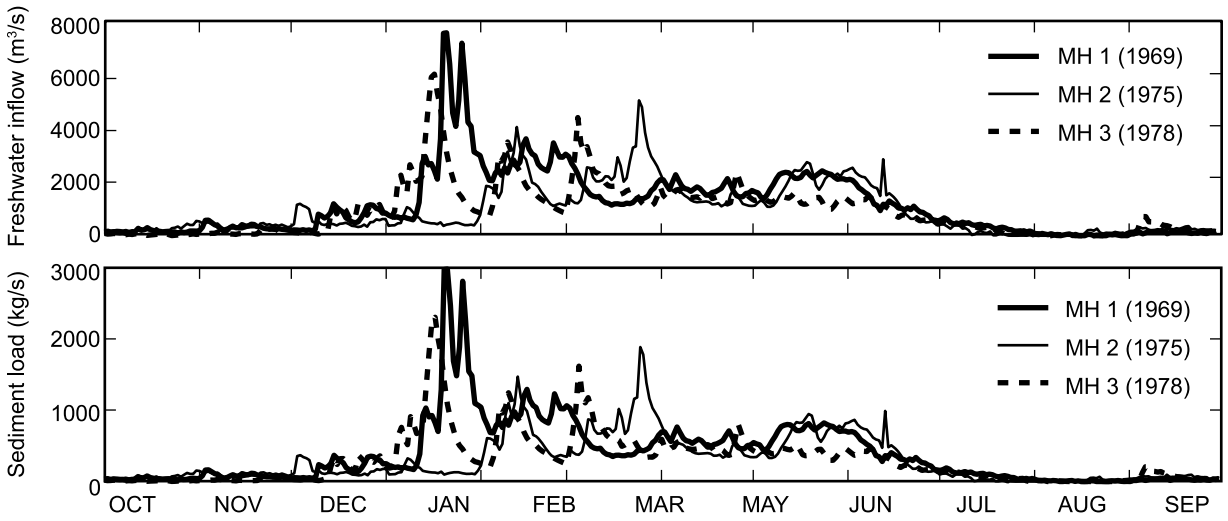

Figure 3. Freshwater flows and sediment loads for the three morphological hydrographs (MH) over the 1867–1887 period.

1 year, but due to computational expense this was not possible. For stability, bed changes over one time step should not exceed 5–10% of the depth [*van der Wegen and Roelvink*, 2008]; with MF = 20 this rate of change was not approached during preliminary runs.

5.4. Selection of Calibration Goals

[27] *Bras et al.* [2003] point out that predicting "detailed geomorphic expression" is not possible, and that model confirmation should focus on statistical or probabilistic quantities. In order of increasing stringency (and difficulty), three goals are evident: representation of (1) net bathymetric change within the entirety of Suisun Bay over the 1867–1887 period (0.40 m); (2) net bathymetric change in specific depth ranges; and (3) bathymetric change on a model cell-by-cell or profile basis. These goals are addressed in the context of the composite result and then the individual morphological hydrographs. We calibrated to the first goal above (for the composite of the three hydrographs), and investigated performance with regards to goals 2 and 3. Parameters that were varied include critical shear stress, wave period, and bed density. These parameters were chosen due to their influence on sediment transport and vertical accretion. There are no historical values for these parameters that can be applied, therefore we began with reasonable estuarine values.

[28] As an additional metric, we used the Brier Skill Score to evaluate spatial correlation. *Sutherland et al.* [2004] detailed the use of the Brier Skill Score (BSS) with regard to morphological models, including the decomposition of the BSS [*Murphy and Epstein*, 1989]. The total BSS ranges from 1 (perfect prediction) to $-\infty$. A value of zero indicates performance equivalent to the null model, which in this case is no observed bathymetric change. Parameter α is a measure of phase error (i.e., discrete locations of erosion and deposition) and approaches 1 for perfect prediction (analogous to the squared correlation coefficient). Parameter β is a measure of amplitude error; perfect prediction of phase and amplitude gives $\beta = 0$. Parameter γ is a measure of the mean bed change error, averaged over the domain; a value of zero indicates perfect prediction. The BSS will be sensitive to the spatial averaging performed, as channels and shoal locations may change.

6. Results

6.1. Bathymetric Change Induced by Composite Results

6.1.1. Net Bathymetric Change Over Entire Domain

[29] The first result of interest was the composite bathymetric change induced by the three morphological hydrographs, each one used as input for a separate 1 year model

Table 2. Observed Bathymetric Change and Modeled Bathymetric Change for Three Morphological Hydrographs in Depth Intervals of 2 m[a]

Depth Range (m)	Area (km^2)	Observed Change (m)	MH 1 Change (m)	MH 2 Change (m)	MH 3 Change (m)	Mean (m)	Error (m)	Error (%)
0–2	39.50 (45%)	0.25	0.27	0.14	0.20	0.20	−0.05	20%
2–4	15.20 (17%)	0.54	0.89	0.84	0.85	0.86	0.32	59%
4–6	16.60 (19%)	0.27	0.42	0.30	0.31	0.35	0.07	26%
6–8	10.10 (11%)	0.66	0.39	0.37	0.34	0.37	−0.29	44%
8–10	4.15 (5%)	1.13	1.12	1.11	1.09	1.11	−0.02	2%
10–12	1.84 (2%)	1.34	0.53	0.67	0.61	0.60	−0.73	54%
12–14	0.96 (1%)	0.13	−0.91	−0.72	−0.81	−0.81	−0.94	723%
>14	0.24 (<1%)	−0.03	−0.49	−0.37	−0.43	−0.43	−0.39	1300%
Total	88.59	0.40	0.46	0.37	0.40	0.41	0.01	**37%**

[a]MH, morphological hydrographs. Mean error, in bold, is the area-weighted error of the individual depth range errors.

Table 3. Decomposition of Brier Skill Score by Depth Interval, With Proposed BSS Classification of *Sutherland et al.* [2004]

Depth Interval (m)	Percent Area	α	β	γ	BSS	Classification
0–2	45	0.11	0.21	0.003	0.05	Poor
2–4	17	0.51	0.02	0.06	0.54	Excellent
4–6	19	0.06	0.45	<0.001	<0	Bad
6–8	11	0.11	0.19	0.002	0.01	Poor
8–10	5	0.45	0.01	0.009	0.59	Excellent
10–12	2	0.04	0.51	0.01	<0	Bad
12–14	1	0.46	0.62	0.21	0.19	Fair
>14	<1	0.03	0.00	0.53	<0	Bad

run. This composited result represented the assumed 20 year change caused by the full set of hydrographs, which we idealized by using three morphological hydrographs and a morphological acceleration factor of 20.

[30] Total deposition, averaged over the basin, was 0.41 m, as compared to the measured deposition of 0.40 m. Best agreement was achieved by altering sediment distribution and wave period. Initial runs with a spatially uniform fine/coarse (low and high critical shear stress, respectively) distribution showed systemic erosion in deeper channels; once the distribution was rectified to reflect coarser conditions in the channel, bathymetric changes in the channels were more reasonable. Channel areas deeper than 7 m were initialized with 20/80 fine/coarse sediment distribution (as opposed to 40/60 elsewhere). Improving agreement in the majority of Suisun Bay, which is dominated by shallow areas (<4 m), was achieved by varying the constant wave period to 1.425 s; wave height and therefore orbital velocity still vary following equations (9)–(12). *Jones and Monismith* [2008] measured wave periods ranging from 1 to 1.6 s in Suisun Bay. *Ganju and Schoellhamer* [2009] demonstrated the model's sensitivity to wave period: a 10% decrease in wave period resulted in greater sediment flux changes than decreases in any other major parameter (settling velocity, critical shear stress, tidal velocity).

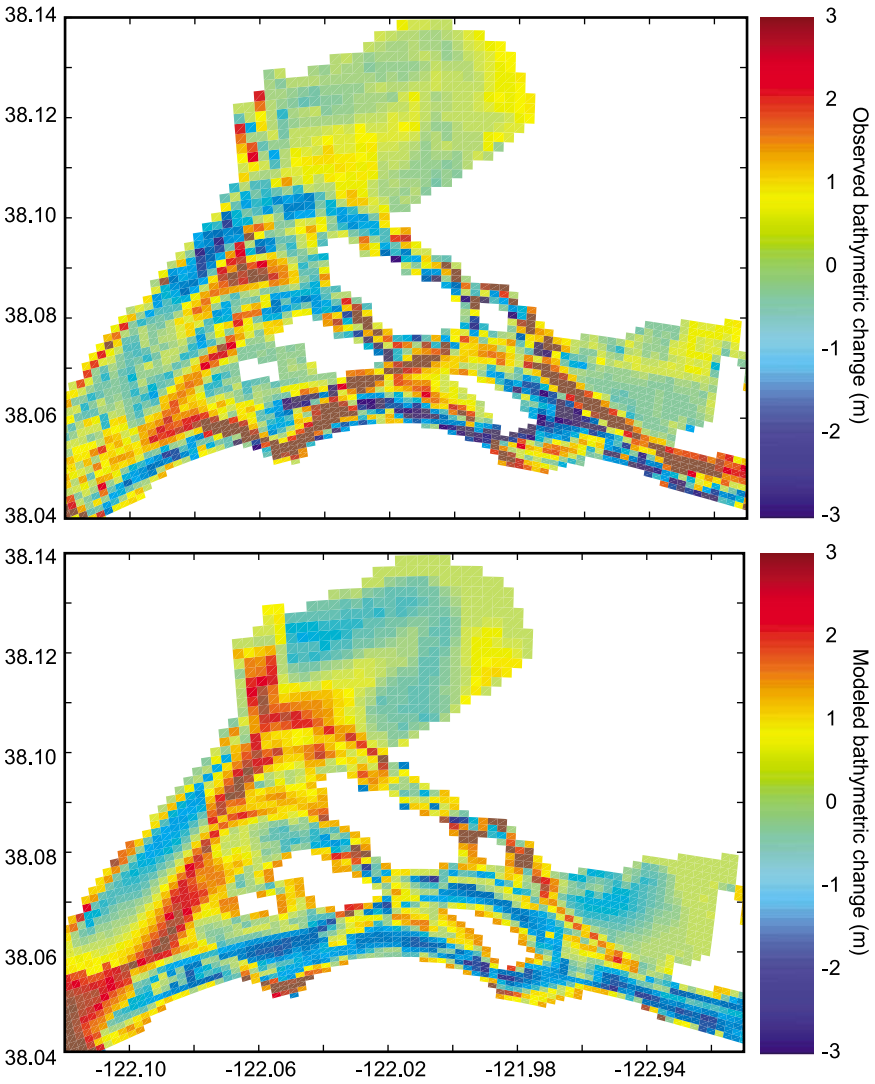

Figure 4. Observed and modeled bathymetric change for 1867–1887 period. Modeled change is the composite results obtained with three morphological hydrographs. Observed change results of *Cappiella et al.* [1999] were interpolated on to the numerical grid used for this study; actual data density is substantially higher.

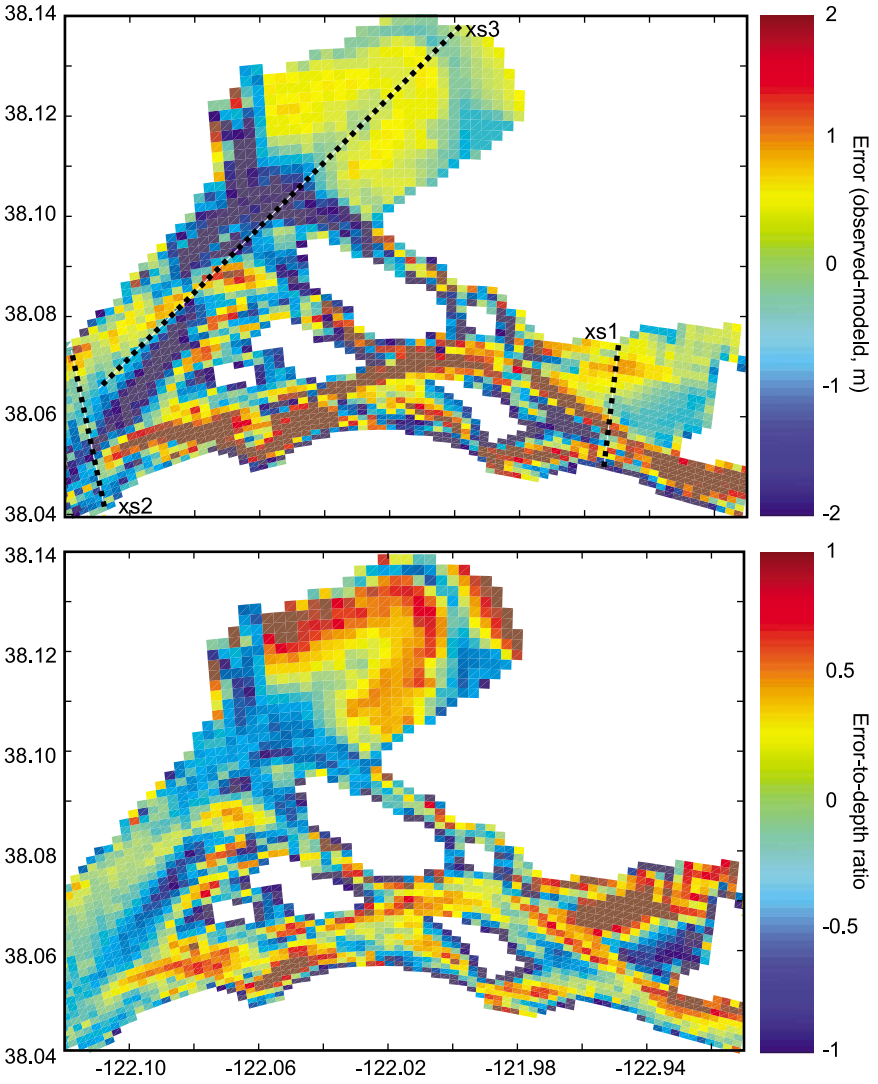

Figure 5. Error between observations and composite model simulation and ratio of error to depth. Positive values indicate underpredicted deposition (or overpredicted erosion); negative values indicate overpredicted deposition (or underpredicted erosion).

6.1.2. Net Bathymetric Change Over Depth Intervals

[31] The composite result of the three morphological hydrographs resulted in a 37% areally weighted error (Table 2). The worst agreement (59% error over 17% of the area) was in the transition zone between channel and shoal (2–4 m): these areas were not as directly susceptible to wind wave resuspension or tidal erosion and were more affected by exchange between shallows and channels. Error in the 2–4 m interval was balanced by overestimated erosion in areas deeper than 6 m. Deeper channels were unaffected by wind wave resuspension; therefore the errors likely represent an imbalance between tidal forcing and initial conditions for bed composition.

[32] The BSS for this effort resulted in scores over 0.5 ("excellent" following *Sutherland et al.* [2004]) for 22% of the area, and scores less than 0.1 ("poor") for 78% of the area (Table 3). However, our calibration goal of representing net bed level changes was met: the value of γ was less than 0.03 for over 80% of the domain. *Sutherland et al.* [2004] achieved an overall value of 0.03 for their morphological simulations; considering the early phase of this type of investigation, this is a useful benchmark.

6.1.3. Bathymetric Change on a Cell-by-Cell or Profile Basis

[33] Major qualitative features that were reproduced include deposition in Grizzly and Honker Bays and erosion in the landward end of the main channel (Figure 4). However, performance for net bathymetric change in Grizzly and Honker Bays was obfuscated by erosional and depositional areas that largely cancel each other (Figure 5). These discrepancies were likely caused by the simplified wind model, which applied a constant wavefield over the entire domain, though bottom orbital velocities (and stresses) were calculated using the updated bathymetry at every time step. The landward section of Honker Bay was less depositional than modeled; this was probably due to the increased fetch under the predominant, westerly wind direction. Properly accounting for the increased fetch would decrease modeled deposition in this area, improving agreement. In Grizzly

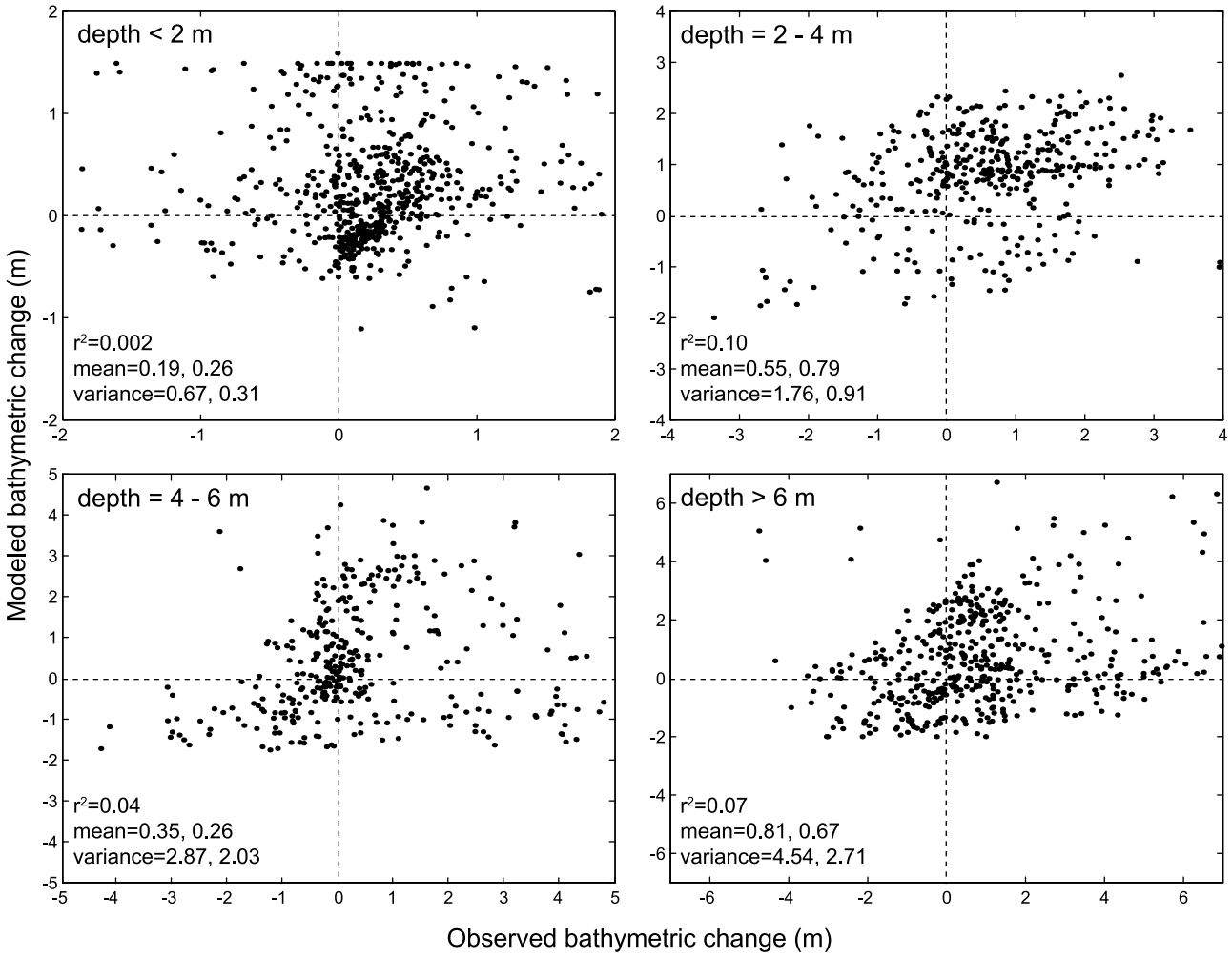

Figure 6. Cell-by-cell comparison, in depth ranges, of observed and modeled bathymetric change for the 1867–1887 period. Means and variances noted are for observations and model simulations, respectively. Mean values differ from values in Table 2 as cell areas are not equal due to curvilinear grid.

Bay, while the phase of erosion and deposition appeared accurate, magnitudes were poorly modeled. *Jones and Monismith* [2008] found that wave breaking for small, short-period waves (<2 s) in Grizzly Bay modulated TKE in the water column; our simplified model did not account for wave breaking which may shift the location and magnitude of maximum erosion in Grizzly Bay.

[34] A cell-by-cell analysis over four depth ranges demonstrates the varying spatial agreement for amplitude (Figure 6). Spatial amplitude correlation was poor, though spatial phase was correctly simulated for 61% of the cells. Variance of bathymetric change increased with depth, and this trend was reproduced by the model, though model variability was damped in comparison to measurements. This pattern is most likely due to migration of the deeper estuarine channels (Figure 4); for example, the landward channel of Suisun Bay accreted over 3 m on the north side and eroded over 3 m on the south side over the 1867–1887 period. Both the spatial error map and cell-by-cell scatterplot demonstrate the difference between spatial correlation for phase and amplitude. While the model was successful for net bathymetric change and prediction of whether a cell is erosional or depositional, performance for the amplitude of those changes was poor.

6.2. Bathymetric Change Anomalies Induced by Each Morphological Hydrograph

6.2.1. Net Bathymetric Change Over Entire Domain

[35] Net deposition expectedly increased with increasing sediment load (Table 4). MH 1, with the largest total sediment load, induced 24% and 15% more deposition than MH 2 and MH 3, respectively, which both prescribed 28% less sediment load than MH 1. The discrepancy between MH 2 and MH 3 is due to the larger peak flow of MH 3; the increased velocity through the idealized delta transported more sediment into Suisun Bay. MH 3 produced the lowest

Table 4. Flow, Sediment Load, and Bed Change Characteristics of Three Morphological Hydrographs

Morphological Hydrograph	Peak Flow (m^3 s^{-1})	Sediment Load (Mt)	Net Bed Change (m)	Mean Absolute Value of Bed Change (m)
1	7553	12.3	0.46	0.87
2	5023	9.6	0.37	0.78
3	5999	9.6	0.40	0.81

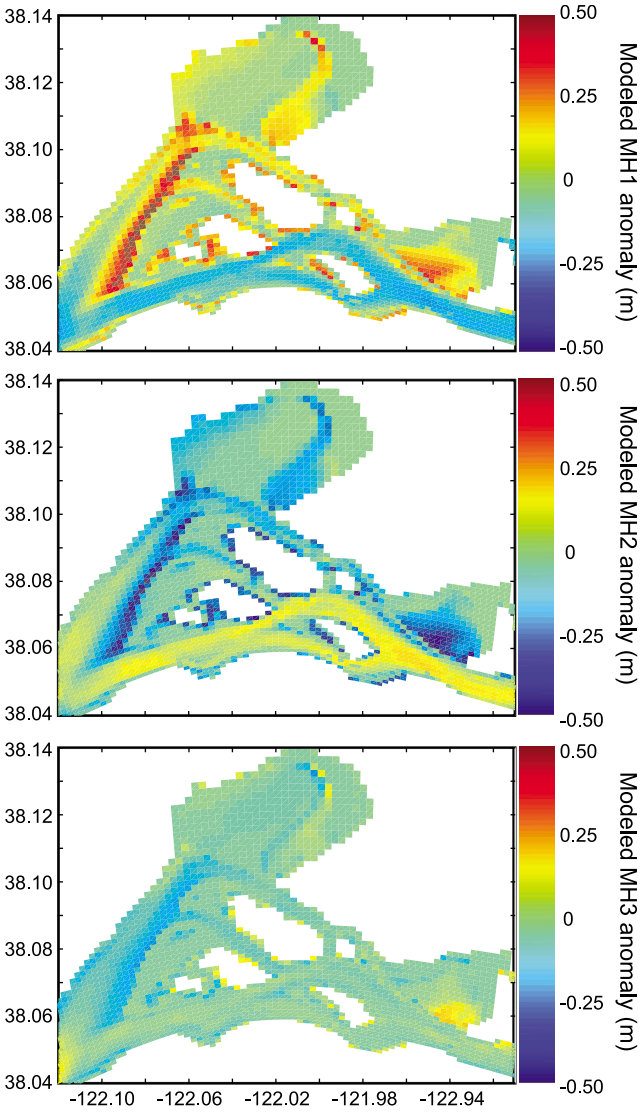

Figure 7. Bathymetric change anomalies for each morphological hydrograph, obtained by differencing individual and composite result. Positive values indicate deposition relative to the composite result, negative values indicate erosion relative to the composite result.

error relative to net bathymetric change (Table 2); this suggests that use of a single, intermediate morphological hydrograph may be sufficient for modeling net basin changes.

6.2.2. Net Bathymetric Change Over Depth Intervals

[36] The largest variability (in terms of normalized standard deviation) in bathymetric change between morphological hydrographs, by depth interval, is seen in the shallowest area (0–2 m). This is again attributed to the difference in total sediment load and peak flows: larger loads induced more deposition, especially in the shallow off-channel areas which were primarily supplied by episodic flows. Larger peak flows, given identical sediment loads (MH 2 versus MH 3) also tended to redistribute sediment from deeper areas to shallower areas (Table 2). All morphological hydrographs produced overestimated erosion in areas greater than 6 m and overestimated deposition in the 2–4 m depth interval. This again points to an imbalance between tidal forcing and initial conditions, which are identical between the three hydrographs.

6.2.3. Bathymetric Change on a Cell-by-Cell or Profile Basis

[37] MH 1 produced greater sediment redistribution than the composite result: channels were relatively more erosional, while deposition was enhanced on the shoulder of the channel that leads northwest from Carquinez Strait to Grizzly Bay, and in Grizzly and Honker Bays (Figure 7). MH 2 produced less redistribution as compared to the mean: main channels were less erosional, and intermediate and shoal areas were less depositional. MH 3 produced changes that were intermediate relative to MH 1 and MH 2. It should be stressed that the relative changes between morphological hydrographs, due to differences in flow timing, are small compared to the overall changes caused by relatively high sediment supply, wind waves, and tidal currents.

[38] The anomaly surfaces, relative to the composite surface, all showed a pronounced curved feature in Grizzly Bay; this feature was essentially the boundary between the subtidal and intertidal domain (Figure 7). Wetting and drying was not activated in the model (see section 7.1), therefore cells ware always active. If a cell deposited enough sediment to break through the water surface, the depth specified to the hydrodynamic module was held just below the water surface to prevent a model crash. The eventual effect was the creation of virtual intertidal areas. The heads of both Grizzly and Honker Bays displayed the creation of virtual intertidal areas, and the curved feature was the intersection between these areas and subtidal areas. Because all three morphological hydrographs produced a similar distribution of virtual intertidal areas, which have final depths of zero relative to mean-lower-low water (Figure 7), the anomalies were equivalent (zero) behind the intersection of subtidal and virtual intertidal areas.

[39] Cross-sectional and longitudinal profiles provide insight into the interaction of hydrodynamic mechanisms with morphological acceleration (Figure 8). On the landward end of Suisun Bay, a cross section from the channel to Honker Bay (xs1, BSS = 0.34) demonstrates the influence of freshwater flow: MH1, with a larger peak flow, induced slightly more erosion on the south side of the channel, and more deposition on the north side toward the entrance to Honker Bay. This suggests that the magnitude of peak freshwater flow is an important redistribution mechanism at the landward end of the estuary. Lack of agreement at the northern end of the cross section, in Honker Bay, suggests that the parameterization of wind wave energy was not spatially accurate, though the average change was predicted well. Conversely, the seaward cross section (xs2, BSS = 0.19) showed little change between hydrographs (and overestimated deposition), as tides had a stronger influence. The third profile, a longitudinal profile from the northwest channel to Grizzly Bay (xs3, BSS = −1.34), showed the poorest agreement between observations and the model. Sediment transport along this transect is influenced mainly by the interaction of tidal forcing, gravitational circulation, and wind wave resuspension [*Schoellhamer and Burau*, 1998]. Given the dependence of gravitational circulation on water depth ($\sim h^3$) and the spring neap cycle, it is possible that a yearly simulation with rapid morphological

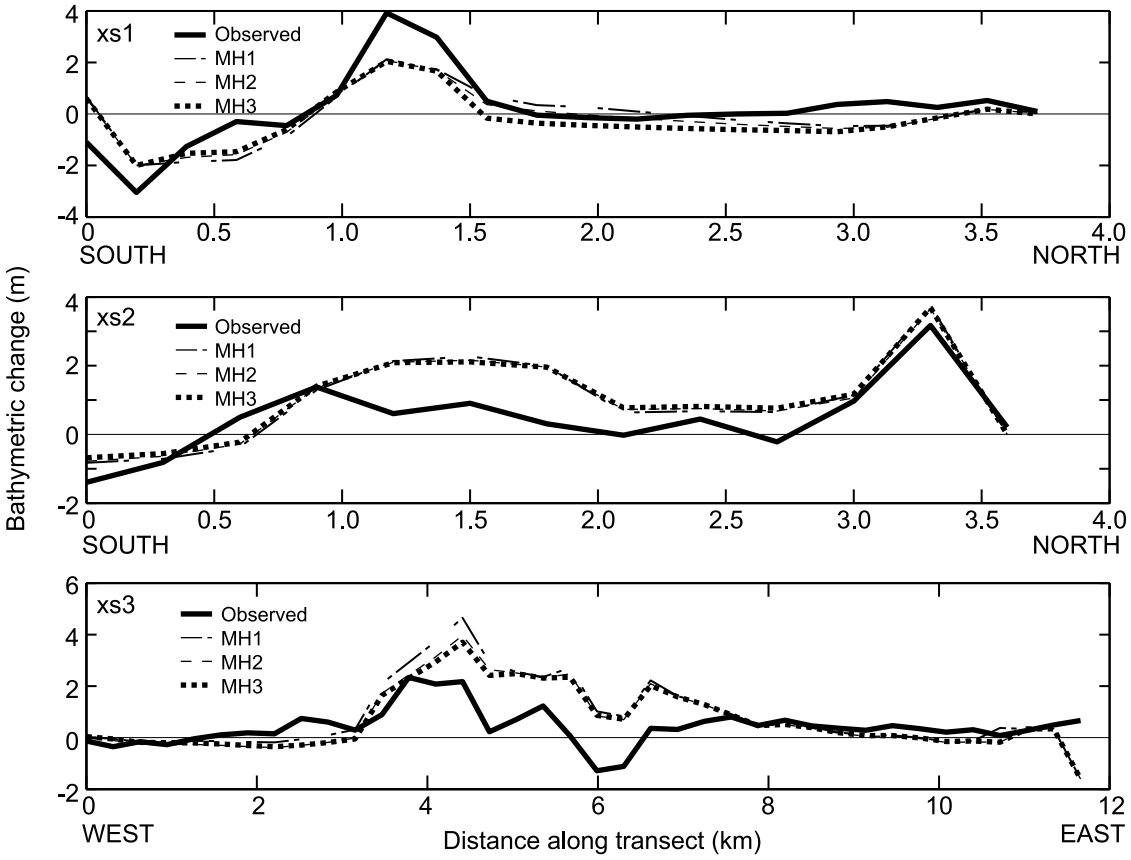

Figure 8. Observed and modeled bathymetric change for each morphological hydrograph along profiles indicated in Figure 5. Skill for composited morphological hydrographs along each profile is 0.34, 0.19, and −1.34, respectively.

acceleration modulates depth at a timescale that does not allow for a realistic depiction of gravitational circulation. On a cell-by-cell basis, the morphological hydrographs showed minimal differences with regard to correlation and variance. This is likely due to identical initial conditions for bed composition, which are of primary importance.

7. Discussion

7.1. Sources of Uncertainty

[40] *Haff* [1996] detailed multiple sources of uncertainty in geomorphic simulations, which are broadly relevant to all modeling endeavors. Exploring these sources in the context of the present modeling endeavor will highlight both strengths and limitations of the present model's formulation and approach.

7.1.1. Model Imperfection

[41] Because of data and computational limitations, we did not apply a wave energy transport model. Considering the limits of grain size data and spatial wind distributions, it is sufficient to use a simple wave model that induces added shear stress on a seasonal basis, in accordance with modern observations. Despite the shortcomings of the wave model (no wave breaking, shoaling, or refraction), it adequately described net changes in the shallowest 2 m of Suisun Bay, where wind wave resuspension is most critical. Poor spatial agreement on a cell-by-cell basis was partially caused by the simplified wind model.

7.1.2. Omission of Processes

[42] Wetting and drying, though a critical process in estuarine systems with intertidal areas, cannot be adequately represented when used in combination with a morphological acceleration factor in an episodic system. Preliminary simulations with the morphological acceleration factor and wetting/drying module indicated a fundamental difficulty in episodic systems, such as Suisun Bay. In the early portion of the simulation, during the episodic sediment delivery by freshwater flow, large depositional features grew in Grizzly and Honker Bays, eventually becoming dry (i.e., land cells). The accelerated morphological change caused these features to grow at a 20-fold rate, as desired. However, as the dry cells were converted to zero-flux boundaries, flow patterns within the shallows were altered, creating minor channels in the shoals that do not appear in the nonwetting/drying simulation. Though the depositional features eroded as the wind wave season commenced, the fundamental changes in channel patterns were noticeable, and did not agree with observations. Allowing fluxes to and from all cells during these simulations was necessary to keep artifacts of this interaction from appearing. This suggests that the use of morphological acceleration, in combination with wetting and drying, may not be possible in episodic systems. The hindcasting results, however, show that disregarding wetting and drying, in a system with 10% intertidal area, is not a major source of error in the shallowest depth interval. In fact, under current trends of intertidal habitat loss [*Jaffe et*

al., 2007], Suisun Bay may not contain intertidal areas by the end of the 21st century. Other work has demonstrated the relationship between coastal armoring and loss of intertidal areas; as sea level rises, intertidal and marsh areas will not be able to retreat landward, due to hardened coasts [*Douglass and Pickel*, 1999].

[43] The exclusion of biotic processes ignores changes in bed density, critical shear stress, and particle size dynamics that may arise through bioturbation and the contribution of organic matter. However, the distribution of benthic communities in an estuarine system can be spatially and temporally variable, and are therefore difficult to quantify. Robust sensitivity analyses, as performed by *Ganju and Schoellhamer* [2009], can be used as a surrogate for unknown benthic processes. For example, if bioturbation tends to decrease critical erosion shear stress, this can be implemented by perturbing the model parameter by a nominal increment and observing model response.

7.1.3. Lack of Initial Condition Information

[44] The historical nature of these simulations highlights the difficulty of specifying initial conditions. Initial conditions are needed for bathymetry, sediment supply (watershed and seaward sources), sediment bed parameters, and estuary configuration. Bathymetry was measured historically, though the quality of these data may not satisfy modern standards. The remaining parameters are not easily quantifiable, and must be used as calibration parameters, estimated using anecdotal evidence, or some combination of the two.

[45] The largest source of error is the specification of grain size distribution, in the lateral as well as vertically (within the bed). Spatial variability of sediment type is high in Suisun Bay (Regional Monitoring Program, Regional monitoring program data access Web site, 2006, http://sfei.org/rmp/rmp_data_access.html), but historical data are not available. The detailed spatial agreement between observations and the model is perhaps most dependent on this initial condition and the vertical distribution of sediment. Even in modern geomorphic modeling applications, these conditions are difficult to specify throughout the domain.

7.1.4. Sensitivity to Initial Conditions

[46] Modeling a system in dynamic equilibrium requires adequate specification of initial conditions. The system being modeled here, however, was in severe disequilibrium due to the catastrophic input of sediment during hydraulic mining. While the simulations may be sensitive to some initial parameters, the major forcings are more dominant than small errors in initial conditions. The exception to this is the aforementioned specification of initial sediment distribution; the trajectory of geomorphic changes at a specific location is highly dependent on the initial bed composition.

7.1.5. Unresolved Heterogeneity

[47] Major parameters that are treated as spatially homogeneous here are wind speed and direction, and sediment bed parameters. Sediment bed parameters are varied between two large portions of the domain (Suisun Bay and the delta), and into two depth regimes. Despite initial unresolved heterogeneity, some characteristics do resolve themselves as the simulation progresses: bed thicknesses and average critical shear stress (mixture of fine/weak and coarse/strong sediment classes) will evolve with time, in response to hydrodynamic forcing.

7.1.6. External Forcing

[48] Perhaps the greatest source of uncertainty is the lack of measured input data. All of the forcing data used here are approximated or idealized in some way, due to the obvious lack of data in the 19th century. Nonetheless, we have attempted to represent key processes, such as wind speed and boundary SSC using modern data. In nonlinear systems, episodic forcing can be the dominant mechanism of interest, and must be quantified. For estuarine hydrodynamic modeling, the main external forcings are tides, freshwater flow, and wind. There are also unknown external processes that can present themselves in an abrupt fashion, such as the dramatic invasion of exotic benthic organisms [*Carlton et al.*, 1990].

7.1.7. Inapplicability of the Safety Factor Concept

[49] In engineered systems, a factor of safety can be introduced to cover the range of possible behaviors. In a natural system, the interaction of heterogeneous materials and variable forcing cannot be scaled with a linear factor of safety. A possible solution is application of a worst-case scenario, though the model will be least reliable when applied to an extreme case outside its calibration space. Between simulation of extreme scenarios and sensitivity analyses, the behavior range of the model should be bracketed in the same sense as a safety factor.

7.2. Mechanism for Bathymetric Change Patterns

[50] The primary mechanism for the net observed and modeled bathymetric change is the increased delivery of watershed sediment during hydraulic mining. Wind wave resuspension and tidal processes are largely responsible for the spatial distribution of bathymetric changes: this is evident from the relatively small changes between morphological hydrographs (due to flow timing), as opposed to the larger changes in net bathymetric change for the composite result. Episodic freshwater flow and sediment delivery tend to scour the main channel and deposit sediment in adjacent intermediate depth (2–6 m) areas. Shoal areas (<2 m) are relatively unaffected by episodic flow peaks, but respond instead to wind wave resuspension. Transfer of sediment between shoal and intermediate depth areas during the wind wave season leads to shoal erosion and intermediate area deposition.

[51] With other forcings held constant, hydrographs with large peak flows tend to cause greater redistribution than years with lower peak flows. The three morphological hydrographs chosen for this hindcasting effort represent typical conditions in terms of flow timing, magnitude, and sediment supply during the late 19th century. However, there are differences between those hydrographs in terms of peak flow, total flow, and total sediment load. Those differences are represented in the bathymetric change anomalies from the composite result for each MH, and the profile from the landward end of the Bay (Figures 7 and 8). In terms of peak flow, MH 1 had the largest peak (Figure 3), followed by MH 3, and MH 2 had the smallest peak. Because of a large flow peak, MH 1 produces greater sediment redistribution than the other morphological hydrographs. Deposition in channel-adjacent areas in Grizzly and Honker Bays is enhanced in the MH 1 simulation, relative to the com-

posite. While wind wave resuspension and tidal currents are the primary forcings, freshwater flow pulses are capable of altering redistribution as well.

8. Conclusions

[52] Hindcasting estuarine bathymetric change is a computationally and data intensive endeavor that requires adequate calibration data, idealization of boundary conditions, and innovative input reduction techniques. In this study we successfully calibrated the ROMS/CSTMS model to decadal-timescale net bathymetric change in Suisun Bay over the 1867–1887 period, with the use of the morphological hydrograph concept and a morphological acceleration factor. Major idealizations included synthetic functions for seaward SSC, wind speed, and salinity. Computational expense was reduced through the use of a morphological acceleration factor that scaled tidal-timescale bed changes by a constant value and updated the bathymetry within the model. Reconstruction of historical freshwater flows and sediment loads led to the identification of a limited set of hydrographs, known as morphological hydrographs, which provide the same bathymetric change as the set of real hydrographs. The model was calibrated to net bathymetric change; error averaged over depth intervals was 37%, while spatial agreement for the amplitude of bathymetric changes was poor. Spatial agreement for the phase of those changes was better, with 61% of the domain correctly indicated as erosional or depositional. Similarly, performance evaluated using the Brier Skill Score suggested better performance in terms of net sediment accretion than spatial amplitude correlation. As the performance criteria became more detailed in a spatial sense, the utility of the model decreased. Therefore the methods are not yet suitable for simulating specific locations of erosion or deposition, but may be useful for estimating basin-scale sedimentation changes.

[53] There are model modifications, such as coarsening the bed in over-erosional areas, that would improve spatial agreement, but these types of modifications cannot be justified without accompanying field data from the period of interest. The decomposed BSS demonstrates the maximum potential the model has with limited intervention (i.e., limited calibration parameters). Further, quantitative comparison for this type of modeling endeavor is exceedingly rare, especially over decadal timescales during the 19th century. While phase correlation is poor over some depth ranges, it is relevant that morphological acceleration and morphological hydrographs can be used in combination to model decadal timescale changes in net sediment accretion and spatial phase correlation (on a cell-by-cell basis) beyond a random estimate (50%).

[54] There are several general findings that can be applied to other estuarine systems. The novel modeling framework, which mandates model calibration to processes over tidal, annual, and decadal timescales, provides a robust tool for simulating geomorphic change in estuaries, especially when computational power and data availability are limited. We established the efficacy of synthetic boundary conditions, morphological acceleration, and the morphological hydrograph in a real estuarine system. Last, it appears that wetting and drying may complicate the use of morphological acceleration in episodic systems. General modeling efforts that require robust calibration, idealized forcing, and input reduction may benefit from the concepts explored in this study.

[55] **Acknowledgments.** This study was supported by the U.S. Geological Survey's Priority Ecosystems Science program, CALFED Bay/Delta Program, and the University of California Center for Water Resources. Use of ROMS and the CSTMS was supported by the U.S. Geological Survey, with assistance from John Warner. This article is contribution 13 to the CASCADE project (Computational Assessments of Scenarios of Change for the Delta Ecosystem, Project SCI-05-C01-84). Any opinions, findings, and conclusions or recommendations expressed in this material are those of the authors and do not necessarily reflect the views of the CALFED Science Program. Input from Dano Roelvink, Mick van der Wegen, anonymous reviewers, and especially the Editor greatly improved the quality of the manuscript.

References

Ariathurai, R., and K. Arulanandan (1978), Erosion rates of cohesive soils, *J. Hydraul. Div. Am. Soc. Civ. Eng.*, *104*, 279–283.

Bras, R. L., G. E. Tucker, and V. Teles (2003), Six myths about mathematical modeling in geomorphology, in *Prediction in Geomorphology*, *Geophys. Monogr. Ser.*, vol. 135, edited by P. R. Wilcock and R. M. Iverson, pp. 63–79, AGU, Washington, D. C.

Buchanan, P. A., and N. K. Ganju (2005), Summary of suspended-sediment concentration data in San Francisco Bay, California, water year 2003, *U.S. Geol. Surv. Data Ser.*, *113*.

Cappiella, K., C. Malzone, R. Smith, and B. Jaffe (1999), Sedimentation and bathymetry changes in Suisun Bay, 1867–1990, *U.S. Geol. Surv. Open File Rep.*, *99-563*.

Carlton, J. T., J. K. Thompson, L. E. Schemel, and F. H. Nichols (1990), Remarkable invasion of San Francisco Bay (California, USA), by the Asian clam *Potamocorbula amurensis*. I. Introduction and dispersal, *Mar. Ecol. Prog. Ser.*, *66*, 81–94, doi:10.3354/meps066081.

Coastal Engineering Research Center (1984), Shore Protection Manual, U.S. Army Corps of Eng., Waterways Exp. Stn., Vicksburg, Miss.

Corenblit, D., A. M. Gurnell, J. Steiger, and E. Tabacchi (2008), Reciprocal adjustments between landforms and living organisms: Extended geomorphic evolutionary insights, *Catena*, *73*, 261–273, doi:10.1016/j.catena.2007.11.002.

Cunge, J. A. (2003), Of data and models, *J. Hydroinf.*, *5*, 75–98.

Dean, R. G., and R. A. Dalrymple (1991), *Water Wave Mechanics for Scientists and Engineers*, 353 pp., World Sci., Singapore.

de Vriend, H. J., M. Capobianco, T. Chesher, H. E. de Swart, B. Latteux, and M. J. F. Stive (1993), Approaches to long-term modelling of coastal morphology: A review, *Coastal Eng.*, *21*, 225–269, doi:10.1016/0378-3839(93)90051-9.

Douglass, S. L., and B. H. Pickel (1999), The tide doesn't go out anymore—The effect of bulkheads on urban bay shorelines, *Shore Beach*, *67*, 19–25.

Droppo, I. G., N. Ross, M. Skafel, and S. N. Liss (2007), Biostabilization of cohesive sediment beds in a freshwater wave-dominated environment, *Limnol. Oceanogr.*, *52*, 577–589.

Escapa, M., D. R. Minkoff, G. M. E. Perillo, and O. Iribarne (2007), Direct and indirect effects of burrowing crab *Chasmagnathus granulatus* activities on erosion of southwest Atlantic *Sarcocornia*-dominated marshes, *Limnol. Oceanogr.*, *52*, 2340–2349.

Ganju, N. K., and D. H. Schoellhamer (2006), Annual sediment flux estimates in a tidal strait using surrogate measurements, *Estuarine Coastal Shelf Sci.*, *69*, 165–178, doi:10.1016/j.ecss.2006.04.008.

Ganju, N. K., and D. H. Schoellhamer (2008), Lateral variability of the estuarine turbidity maximum in a tidal strait, in *Sediment and Ecohydraulics: INTERCOH 2005*, edited by T. Kusuda et al., pp. 339–355, Elsevier, Amsterdam. (Available at http://ca.water.usgs.gov/mud/publications/ganju_schoellhamer_ETM.pdf)

Ganju, N. K., and D. H. Schoellhamer (2009), Calibration of an estuarine sediment transport model to sediment fluxes as an intermediate step for robust simulation of geomorphic evolution, *Cont. Shelf Res.*, *29*, 148–158, doi:10.1016/j.csr.2007.09.005.

Ganju, N. K., N. Knowles, and D. H. Schoellhamer (2008), Temporal downscaling of decadal sediment load estimates to a daily interval for use in hindcast simulations, *J. Hydrol.*, *349*, 512–523, doi:10.1016/j.jhydrol.2007.11.026.

Gilbert, G. K. (1917), Hydraulic mining debris in the Sierra Nevada, *U.S. Geol. Surv. Prof. Pap.*, *105*, 148 pp.

Haff, P. K. (1996), Limitation on predictive modeling in geomorphology, in *The Scientific Nature of Geomorphology*, edited by B. L. Rhoads and C. E. Thorn, pp. 337–358, John Wiley, New York.

Hibma, A., H. J. de Vriend, and M. J. F. Stive (2003), Numerical modeling of shoal pattern formation in well-mixed elongated estuaries, *Estuarine Coastal Shelf Sci.*, *57*, 981–991, doi:10.1016/S0272-7714(03)00004-0.

Jaffe, B. E., R. E. Smith, and A. C. Foxgrover (2007), Anthropogenic influence on sedimentation and intertidal mudflat change in San Pablo Bay, California: 1856–1983, *Estuarine Coastal Shelf Sci.*, *73*, 175–187, doi:10.1016/j.ecss.2007.02.017.

Jones, N. L., and S. G. Monismith (2008), The influence of whitecapping waves on the vertical structure of turbulence in a shallow estuarine embayment, *J. Phys. Oceanogr.*, *38*, 1563–1580, doi:10.1175/2007JPO3766.1.

Knowles, N. (2002), Natural and human influences on freshwater inflows and salinity in the San Francisco Estuary at monthly to interannual scales, *Water Resour. Res.*, *38*(12), 1289, doi:10.1029/2001WR000360.

Krone, R. B. (1979), Sedimentation in the San Francisco Bay system, in *San Francisco Bay: The Urbanized Estuary*, edited by T. J. Conomos, pp. 85–96, Pac. Div., Am. Assoc. for the Adv. of Sci., San Francisco, Calif.

Latteux, B. (1995), Techniques for long-term morphological simulation under tidal action, *Mar. Geol.*, *126*, 129–141, doi:10.1016/0025-3227(95)00069-B.

Lesser, G. R., J. A. Roelvink, J. A. T. M. van Kester, and G. S. Stelling (2004), Development and validation of a three-dimensional morphological model, *Coastal Eng.*, *51*, 883–915, doi:10.1016/j.coastaleng.2004.07.014.

Madsen, O. S. (1994), Spectral wave-current bottom boundary layer flows, paper presented at 24th International Conference, Coastal Eng. Res. Counc., Kobe, Japan.

Meko, D. M., M. D. Therrell, C. H. Baisan, and M. K. Hughes (2001), Sacramento River flow reconstructed to A. D. 869 from tree rings, *J. Am. Water Resour. Assoc.*, *37*, 1029–1039, doi:10.1111/j.1752-1688.2001.tb05530.x.

Meko, D. M., R. Touchan, M. Hughes, and A. C. Caprio (2002), San Joaquin River flow reconstructed from tree rings, in *Proceedings of the 19th Annual Pacific Climate Workshop*, edited by G. J. West and N. L. Blomquist, *Estuary Tech. Rep. 71*, p. 186, Interagency Ecol. Program, San Francisco, Calif.

Murphy, A. H., and E. S. Epstein (1989), Skill scores and correlation coefficients in model verification, *Mon. Weather Rev.*, *117*, 572–581, doi:10.1175/1520-0493(1989)117<0572:SSACCI>2.0.CO;2.

Oreskes, N., K. Shrader-Frechette, and K. Belitz (1994), Verification, validation, and confirmation of numerical models in the earth sciences, *Science*, *263*, 641–646, doi:10.1126/science.263.5147.641.

Porterfield, G. (1980), Sediment transport of streams tributary to San Francisco, San Pablo, and Suisun bays, California, 1909–1966, *U.S. Geol. Surv. Water Resour. Invest., 80-64*, 92 pp.

Roache, P. J. (1997), Quantification of uncertainty in computational fluid dynamics, *Annu. Rev. Fluid Mech.*, *29*, 123–160, doi:10.1146/annurev.fluid.29.1.123.

Roelvink, J. A. (2006), Coastal morphodynamic evolution techniques, *Coastal Eng.*, *53*, 277–287, doi:10.1016/j.coastaleng.2005.10.015.

Schoellhamer, D. H., and J. R. Burau (1998), Summary of findings about circulation and the estuarine turbidity maximum in Suisun Bay, California, *U.S. Geol. Surv. Fact Sheet, FS-047-98*, 6 pp.

Schoellhamer, D. H., N. K. Ganju, P. R. Mineart, and M. A. Lionberger (2008), Sensitivity and spin up times of cohesive sediment transport models used to simulate bathymetric change, in *Sediment and Ecohydraulics: INTERCOH 2005*, edited by T. Kusuda et al., pp. 463–475, Elsevier, Amsterdam. (Available at http://ca.water.usgs.gov/mud/publications/Schoellhamer_et_al.pdf)

Shchepetkin, A. F., and J. C. McWilliams (2005), The Regional Ocean Modeling System (ROMS): A split-explicit, free-surface, topography-following coordinates ocean model, *Ocean Modell.*, *9*, 347–404, doi:10.1016/j.ocemod.2004.08.002.

Sutherland, J., A. H. Peet, and R. L. Soulsby (2004), Evaluating the performance of morphological models, *Coastal Eng.*, *51*, 917–939, doi:10.1016/j.coastaleng.2004.07.015.

Thompson, J. (1957), The settlement geography of the Sacramento-San Joaquin Delta, California, Ph.D. dissertation, Stanford Univ., Stanford, Calif.

Umlauf, L., and H. Burchard (2003), A generic length-scale equation for geophysical turbulence models, *J. Mar. Res.*, *61*, 235–265, doi:10.1357/002224003322005087.

van der Wegen, M., and J. A. Roelvink (2008), Long-term morphodynamic evolution of a tidal embayment using a two-dimensional, process-based model, *J. Geophys. Res.*, *113*, C03016, doi:10.1029/2006JC003983.

Wahba, G. (1990), *Spline models for observational data*, 169 pp., Soc. for Ind. and Appl. Math., Philadelphia, Pa.

Warner, J. C., D. H. Schoellhamer, C. A. Ruhl, and J. R. Burau (2004), Floodtide pulses after low tides in shallow subembayments adjacent to deep channels, *Estuarine Coastal Shelf Sci.*, *60*, 213–228, doi:10.1016/j.ecss.2003.12.011.

Warner, J. C., W. R. Geyer, and J. A. Lerczak (2005a), Numerical modeling of an estuary: A comprehensive skill assessment, *J. Geophys. Res.*, *110*, C05001, doi:10.1029/2004JC002691.

Warner, J. C., C. R. Sherwood, H. G. Arango, and R. P. Signell (2005b), Performance of four turbulence closure models implemented using a generic length scale method, *Ocean Modell.*, *8*, 81–113, doi:10.1016/j.ocemod.2003.12.003.

Warner, J. C., C. R. Sherwood, R. P. Signell, C. K. Harris, and H. G. Arango (2008), Development of a three-dimensional, regional, coupled wave-, current-, and sediment-transport model, *Comput. Geosci.*, *34*, 1284–1306, doi:10.1016/j.cageo.2008.02.012.

N. K. Ganju, U.S. Geological Survey, 384 Woods Hole Rd., Woods Hole, MA 02543-1598, USA. (nganju@usgs.gov)

B. E. Jaffe, U.S. Geological Survey, 400 Natural Bridges Dr., Santa Cruz, CA 95060, USA. (bjaffe@usgs.gov)

D. H. Schoellhamer, U.S. Geological Survey, Placer Hall, 6000 J St., Sacramento, CA 95819, USA. (dschoell@usgs.gov)